# Thermal and mechanical properties of Mg–Al–Si–O–N glasses with up to 6.2 at.% nitrogen

Theany To, Chouaib Mhamdia, Sharafat Ali, Patrick Houizot, Karolina Milewska, Franck Tessier, Alain Moréac, Tanguy Rouxel

Received: 12 December 2024 | Revised: 15 January 2025 | Accepted: 16 February 2025

DOI: 10.1111/jace.20487

Journal of the American Ceramic Society

RESEARCH ARTICLE

# Thermal and mechanical properties of Mg–Al–Si–O–N glasses with up to 6.2 at.% nitrogen

**Theany To**[1] | **Chouaib Mhamdia**[1] | **Sharafat Ali**[2] | **Patrick Houizot**[1] | **Karolina Milewska**[2] | **Franck Tessier**[3] | **Alain Moreac**[1] | **Tanguy Rouxel**[1,4]

[1]Univ Rennes, CNRS, IPR (Institut de Physique de Rennes) - UMR 6251, Rennes, France

[2]Department of Built Environment and Energy Technology, Linnaeus University, Växjö, Sweden

[3]Univ Rennes, CNRS, ISCR (Institut des Sciences Chimiques de Rennes) - UMR 6226, Rennes, France

[4]Institut Universitaire de France (IUF), Rennes, France

**Correspondence**
Theany To, Univ Rennes, CNRS, IPR (Institut de Physique de Rennes) - UMR 6251, F-35000 Rennes, France.
Email: theany.to@univ-rennes.fr

Sharafat Ali, Department of Built Environment and Energy Technology, Linnaeus University, Växjö, Sweden.
Email: sharafat.ali@lnu.se

**Funding information**
Carl Tryggers Stiftelse för Vetenskaplig Forskning, Grant/Award Number: CTS 23:2732; European Union's Horizon 2020 research and innovation program under the Marie Skłodowska-Curie grant agreement, Grant/Award Number: 899546

**Abstract**

This study investigates the structural, thermal, and mechanical properties of Mg–Al–Si–O–N glasses. Six compositions with increasing nitrogen content from 1.7 to 6.2 at.% were synthesized by melting mixtures of high-purity oxide and nitride precursors, followed by quenching and annealing. Structural analysis via X-ray diffraction and Raman spectroscopy confirms the amorphous nature of the glasses and highlights distinct spectral features based on the Mg/Al ratios, providing insight into the changes of the Si-O and Al-O bond concentration with the nitrogen content. The effects of nitrogen incorporation on density, molar volume, atomic packing density, glass transition temperature, and thermal expansion were systematically examined, revealing strong correlations. Measurements of elastic moduli, hardness, and fracture toughness underscore the role of nitrogen and the Mg/Al ratio in enhancing the mechanical properties. The findings demonstrate that by increasing the nitrogen content, the glass becomes stiffer and denser, and the mechanical properties are improved.

**KEYWORDS**
elastic property, fracture toughness, glass structure, oxynitride glass, SEPB

## 1 | INTRODUCTION

Oxynitride glasses, in which nitrogen replaces oxygen in the glass network, represent a significant advancement in materials science due to their unique structure and superior properties. Compared to oxide glasses, oxynitride glasses exhibit enhanced chemical durability, hardness, fracture toughness, refractive index, and thermal stability, giving them a high potential for structural applications. The incorporation of nitrogen into glass matrices strengthens the network through the formation of stronger Si–N covalent bonds, which increase rigidity and crosslinking.[1–5] The development of oxynitride glasses with tailored properties has been driven by the need to understand the interplay between composition, structure, and performance. For instance, incorporating nitrogen

increases the glass transition temperature ($T_g$), reduces the coefficient of thermal expansion (*CTE*), and enhances some mechanical properties such as hardness and elastic moduli.[6–16]

Investigations on M-(Al)-Si-O-N and related systems have explored the glass-forming regions and composition-property relationships. The structure of oxynitride glass have primarily been probed by X-ray and neutron diffraction,[17–19] IR and Raman spectroscopy,[20–24] XPS,[24–27] and solid-state NMR techniques.[7,18,21,28–31] Studies of M-(Al)-Si-O-N glasses have revealed that nitrogen content, cation type, and the molar ratios of M, Si, and Al critically influence the physical properties. For example, nitrogen strengthens the network by replacing $O^{[2]}$ linkages with $N^{[3]}$ sites, leading to a more rigid and more interconnected structure. In M–(Al)–Si–O–N glasses, the cross-linking degree of $Si(ON)_4$ and $Al(ON)_4$ tetrahedra, as well as the cation–anion bond strengths, play a crucial role in determining thermal, mechanical, and elastic properties. Furthermore, the configuration of aluminum in oxide and oxynitride glass networks may involve Al in higher coordination states, such as $AlO_5$ and $AlO_6$ polyhedra, corresponding to $Al^{[5]}$ and $Al^{[6]}$ species. These configurations may either act as network formers (tetrahedrally coordinated by oxygen) or as modifiers in five- or six-fold coordination.[3,29,32]

Among alkaline-earth systems, Ca-(Al)-Si-O-N glasses have been the most extensively studied, but other compositions, such as those containing Mg,[33–38] Sr,[14,39] and Ba,[40–42] are also gaining attention. Studies on the formation of Mg–Al–Si–O–N and related glasses typically involve melting Si and/or Al oxides and nitrides in a nitrogen atmosphere, followed by a melt-quench process to produce glasses with nitrogen contents reaching approximately 7 atomic percent, or about 16 equivalent percent (eq.%) of nitrogen among the total anions (O and N). Alternatively, substantially nitrogen-richer glasses, with nitrogen contents of up to approximately 38 atomic percent (or 68 eq.%), can be produced using metal hydrides or metallic precursors,[37,39,42–45] particularly in systems like Ca–Si–O–N[43,45–49] and Sr–Si–O–N.[37,39,50] Additionally, oxynitride glasses are generally not transparent within the visible spectrum,[1,5,11,45,51–57] making the production of optically transparent M–(Al)–Si–O–N glasses with high nitrogen content a significant challenge.

However, while oxynitride glasses offer significant advantages, the understanding of their structure-property relationships remains limited. This study aims to provide a detailed understanding of these relationships in Mg–Al–Si–O–N glasses, focusing on the effects of nitrogen content and Mg/Al ratios on network rigidity and physical properties. Additionally, this study seeks to develop regression models that could potentially predict the performance of similar glass systems. Raman spectroscopy was employed to analyze structural configurations, complemented by measurements of density, molar volume, compactness, hardness, elastic moduli (including Young's modulus, bulk modulus, and shear modulus), crack resistance, and fracture toughness. These insights will serve as a predictive framework for designing high-performance oxynitride glasses tailored for advanced technological applications.

**TABLE 1** Actual glass composition ± at.%.

| ref. | Mg | Al | Si | O | N | N/O | Mg/Al | Al/Si |
|---|---|---|---|---|---|---|---|---|
| $N_{1.7}$ | 7.0 | 9.7 | 20.9 | 60.7 | 1.7 | 0.030 | 0.722 | 0.464 |
| $N_{3.6}$ | 6.7 | 9.7 | 21.2 | 58.8 | 3.6 | 0.061 | 0.691 | 0.458 |
| $N_{4.9}$ | 6.5 | 9.1 | 22.2 | 57.3 | 4.9 | 0.086 | 0.714 | 0.410 |
| $N_{5.7}$ | 4.4 | 9.5 | 23.4 | 57.0 | 5.7 | 0.100 | 0.463 | 0.406 |
| $N_{5.8}$ | 5.9 | 10.3 | 21.7 | 56.3 | 5.8 | 0.103 | 0.573 | 0.475 |
| $N_{6.2}$ | 5.5 | 12 | 20.7 | 55.6 | 6.2 | 0.112 | 0.458 | 0.580 |

## 2 | EXPERIMENTAL

A list of the Mg–Al–Si–O–N glasses considered herein is presented in Table 1 labeled "$N_n$," where *n* refers to the at.% of N. For all $N_n$ glasses, 500 g of high-purity oxide precursors of MgO, $SiO_2$, $Al_2O_3$, and AlN (>99.99 %, ChemPure) were ball-milled. The mixture was then melted by heating in a sealed quartz tube, up to around 1650°C. The melt was held for 90 min before quenching into a preheated graphite mold. The obtained glass sample was annealed for 2 h at $T_g$ − 50°C to reduce the internal stresses without inducing significant crystal nucleation.

The composition of glasses in Table 1 was verified by means of energy dispersive spectroscopy (EDS) in a scanning electron microscope (SEM) and with the determination of the N content using a LECO TC-600 analyzer.

Raman spectra were recorded in the range of 400–1300 with a 1.7 $cm^{-1}$•$px^{-1}$ dispersion that corresponds to a spectral resolution around 5 $cm^{-1}$, using a micro-Raman spectrometer (HR-Evo, Horiba Scientific). A 532-nm green diode laser was used to excite the sample surface for an acquisition time of 10 s. No heating effect has been observed. At least two spectra from two different locations on the glass were recorded for each specimen. The spectra were subjected to baseline subtraction and normalization with respect to their area.

Dilatometry (L75 Paltinum, Linseis) was performed to measure the linear thermal expansion coefficients (*CTE*) and the glass transition temperature ($T_g$). The measurement was carried out on rectangular rods of 4×4×15 $mm^3$, heating at a rate of 5°C $min^{-1}$ in ambient atmosphere from room temperature to 1000°C. The measured data were calibrated with the one of the alumina rods with the same

dimension. $T_g$ was derived from the thermal expansion curve as the temperature at the point of intersection of the linear sections below (from 300°C) and above $T_g$. The precision of the $T_g$ measurements was estimated to be 5°C. *CTE* was calculated by

$$CTE = \frac{dL}{L_0 dT}, \tag{1}$$

where $dL$, $L_0$, and $dT$ represent the elongation under heating, the original length of the specimen, and the temperature change, respectively. The error of the measure was $\pm 0.1\times10^{-6}$ $K^{-1}$.

Density ($\rho$) was measured by the Archimedes method on glass sample of about 5×10×10 $mm^3$ in distilled water at 22°C. The average density and its standard deviation ($\pm$ 0.005 g $cm^{-3}$) of each glass were obtained from at least five repetitions of three different pieces of each glass sample. The density data were further used to estimate the molar volume ($V_M$) and the atomic packing density ($C_g$) as

$$V_M = \frac{\sum_i x_i M_i}{\rho}, \tag{2}$$

$$C_g = N_A \frac{\sum_i (4/3)\pi x_i r_i^3}{V_M}, \tag{3}$$

where $x_i$, $M_i$, and $r_i$ are the atomic fraction, ionic radius, and the molar mass of element $i$, respectively, and $N_A$ is the Avogadro's number. In this study, we used the Shannon–Prewitt ionic radii[58] for the following (average) coordination numbers $\{Z_{Mg}, Z_{Al}, Z_{Si}, Z_O, Z_N\} = \{7, 4, 4, 2, 4\}$ throughout the calculation. The uncertainty for $V_M$ and $C_g$ are estimated to be $\pm$ 0.02 $cm^3$ $mol^{-1}$ and $\pm$ 0.005, respectively.

Elastic moduli were determined at ambient atmosphere on cut and polished glass samples of about 5×10×10 $mm^3$ by means of ultrasonic echography using 10 MHz piezoelectric transducers in contact with the glass sample via a coupling gel. Young's modulus ($E$), shear modulus ($G$), Poisson's ratio ($\nu$), and bulk modulus ($K$) were derived from the acoustic wave velocity and from the calculated glass density using the following expressions:

$$E = \rho \frac{3V_L^2 - 4V_T^2}{\left(\frac{V_L}{V_T}\right)^2 - 1}, \tag{4}$$

$$G = \rho V_T^2, \tag{5}$$

$$\nu = \frac{E}{2G} - 1, \tag{6}$$

$$K = \frac{E}{3(1-2\nu)}, \tag{7}$$

where $V_L$ and $V_T$ are the longitudinal and transversal wave velocities, respectively.

Hardness ($H$) and the crack initiation resistance ($CR$) were determined by using Vickers indentation (Matsuzawa VMT-7S) at ambient atmosphere with a stepwise increasing load ($P_{ind}$) from 2.9 to 49.1 N. The loading/unloading duration as well as the dwell time were set to 15 s. For each indentation load, 20 indents were made on each glass sample, and $H$ is expressed as the ratio of the load on the projected imprint area as

$$H = \frac{2P_{ind}}{d^2}, \tag{8}$$

where $d$ is an average of two diagonal lengths of an indent. $CR$ is the indentation load, at which 50% crack probability is recorded.[59] For a Vickers indenter, the crack probability is 100%, 75%, 50%, 25%, and 0% when there are four, three, two, one, and zero (radial/median type) corner cracks, respectively.

Fracture toughness ($K_{Ic}$) was determined by means of the single-edge precracked beam (SEPB) method following Ref. 60. First, the glass was cut and polished to have the breadth ($B$) of 3 $\pm$ 0.1 mm, the width ($W$, also called the "height") of 4 $\pm$ 0.1 mm, and the length ($L$) of 25 $\pm$ 2 mm. A line of Vickers indents (9.8 N) was created along the middle of the length $L$, and on the side $B$ with a distance of 150 μm from one indent to another. The indented specimen was then set in a bridge-compression fixture.[60,61] The indented surface was positioned over the lower support by carefully assuring that the indentation line was in the middle of the groove (side in tension). Since the glass specimens were not transparent to the naked eyes, and thus to reassure the position of the indentation line in the groove side, a mirror was put in the groove of the lower support (under the indentation line) and a camera was used to observe this. When the compressive load was applied, the lower part of the specimen was put in tension thanks to the groove of the lower support, and thus, the upper part of the specimen was in compression. The tension allowed the crack to propagate from the indentation line until it reached the compressive stress of the upper part of the specimen, where the crack stopped. This bridge-compression fixture allows to have a precracked specimen with the crack length ($a$) of about half of $W$. Finally, the precracked specimen was fractured in three-point bending experiment. The distance of the two support rollers ($S$) is 20 $\pm$ 0.001 mm. To minimize the stress corrosion phenomena, a cross-head speed of 15 μm $s^{-1}$ was used as in Refs. 60 and 61. The fracture toughness was then calculated from the peak load ($P_{max}$) of the three-point bending test as[60,62]

$$K_{Ic} = \frac{P_{max}}{BW^{0.5}} Y^* \text{with } Y^* = \frac{3}{2}\frac{S}{W}\frac{\alpha^{0.5}}{(1-\alpha)^{1.5}} f(\alpha), \tag{9}$$

where $f(\alpha) = 1.9109 - 5.1552\alpha + 12.6880\alpha^2 - 19.5736\alpha^3 + 15.9377\alpha^4 - 5.1454\alpha^5$, and $\alpha$ is the ratio of $a \bullet W^{-1}$.

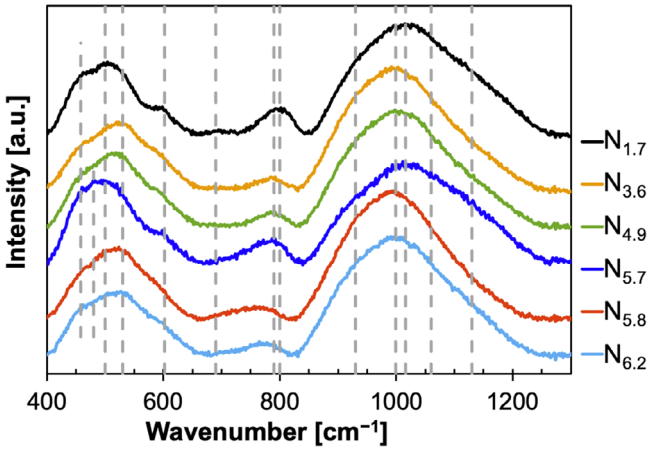


**FIGURE 1** Normalized and background-corrected Raman spectra for all the glass samples.

## 3 | RESULTS AND DISCUSSION

### 3.1 | Glass formation and structure

The analyzed composition of the six studied glasses is given in Table 1. During the melting process, nitrogen content may vary, leading to deviations from the set composition parameters. In this study, the actual composition is used for the analysis. A series of compositions with increasing nitrogen content, from 1.7 to 6.2 at.% was synthesized. Broad humps are observed for all glasses by XRD, which confirms the amorphous nature of the studied material to X-rays. The obtained glass appears to be macro- and microscopically homogenous, bubble-free, and optically translucent in the visible range, but slightly tinted dull gray.

The Raman spectra for all glass composition are shown in Figure 1. In these spectra, three obvious peaks appear in the wavenumber ranges of 400–650 $cm^{-1}$ (the low-frequency region), 650–850 $cm^{-1}$ (the midfrequency region), and 850–1300 $cm^{-1}$ (the high-frequency region). However, to make it convenient, we divide the Raman spectra analysis into two main parts: the per-alkaline earth samples (i.e., $N_{1.7}$, $N_{3.6}$, $N_{4.9}$, and $N_{5.8}$ that have 2Mg/Al > 1) and the per-alumina samples ($N_{5.7}$ and $N_{6.2}$, for which 2Mg/Al < 1).

**Per-alkaline earth** ($N_{1.7}$, $N_{3.6}$, $N_{4.9}$, and $N_{5.8}$): The glasses show maximum peaks in the 850–1300 $cm^{-1}$ range, which corresponds to the asymmetric stretching modes of $Q^2$, $Q^3$, and $Q^4$ silica units.[63,64] Here, $Q^2$ and $Q^3$ represent silicate tetrahedra units with two and one nonbridging oxygens (NBOs), respectively, while $Q^4$ is the fully cross-linked silicate structure with four bridging oxygens (BOs). In literature, $Q^2$, $Q^3$, and $Q^4$ are associated to the bands at 950, 1100, and 1150 $cm^{-1}$, while the 1050 $cm^{-1}$ band is attributed for Si-O vibrations of structural species containing BO with either complete polymerization or those with alkali metals.[63,64] A study on the MgAlSiO glasses shown that the latter peak (also a maximum peak) is at over 1050 $cm^{-1}$ for the sample with 2Mg/Al = 1 and is below 1016 $cm^{-1}$ for the 2Mg/Al = 3.[64] In our case, $N_{1.7}$, having 2Mg/Al = 1.44, shows the maximum broad peak at 1020 $cm^{-1}$, with a left shoulder at ~950 $cm^{-1}$ and right shoulders at ~1100 and 1150 $cm^{-1}$ as in the literature.[63,64] For oxynitride glasses and for the per-alkaline earth glass samples ($N_{1.7}$, $N_{3.6}$, $N_{4.9}$, and $N_{5.8}$ in Figure 1), the peak maxima decrease, with decreasing the alkaline earth Mg content (i.e., the increase of N content), from 1020 to 990 $cm^{-1}$. Sample $N_{5.8}$, having the lowest Mg content, shows the maximum peak at 990 $cm^{-1}$ with a clear left shoulder at 930 $cm^{-1}$, and lower right shoulder comparing to sample $N_{1.7}$. This shift to longer wavelengths shows the superposition of $Si(OAl)_z$ units, where z is the number of $AlO_4$ tetrahedra connected to a $SiO_4$ one, resulting from substituting $Al^{3+}$ for $Si^{4+}$, which is in good agreement with both concepts of a reduction in force constant and to (Al, Si) coupling.[64–68]

A distant peak near 800 $cm^{-1}$ is observed in the $N_{1.7}$ sample (Figure 1), attributed to the cage motion of O-Si-O stretching vibration.[69] In our study, the peak of this band broadens, shifts to lower frequencies, and decreases in intensity with decreasing the Mg content. The decrease of Mg content leads to the shortage of $Mg^{2+}$ to compensate the charge of $Si^{4+}$, resulting in the relatively lower BOs of $SiO_4$ comparing to those of $AlO_4$. As an example, sample $N_{5.8}$, having the lowest 2Mg/Al = 1.15, shows the maximum peak at 760 $cm^{-1}$ with import shoulder at ~700 $cm^{-1}$, which is corresponding to the $AlO_4$ polyhedra.[70] The broadening, shifting, and lowering intensities of this band was also observed in the MgAlSiO glasses with increasing Mg content (and decreasing Si content).[64] In the low-frequency region (i.e., 400–650 $cm^{-1}$), sample $N^{1.7}$ shows the maximum peak at 500 $cm^{-1}$, with a shoulder at 458 $cm^{-1}$ and a small peak at 600 $cm^{-1}$. The decrease of Mg content results in the shift of the maximum peak to higher frequency (at ~530 $cm^{-1}$) with lowering the shoulder at 458 $cm^{-1}$. Again, this shift of the maximum peak to low wavelength and the superposition of several components including the bands at 530 and 600 $cm^{-1}$ were also observed in the MgAlSiO glasses when increasing the Mg content (i.e., decreasing the Si/Al ratio).[64] These bands are associated with the motions of BO in Si-O-Si and Si-O-Al.[65,66]

**Per-alumina samples** ($N_{5.7}$ and $N_{6.2}$, for which 2Mg/Al < 1): $N_{5.7}$ sample, having the largest silica content (i.e., the highest Si/Al = 2.46), shows a broad maximum peak at 1020 $cm^{-1}$, with a left shoulder at 900 $cm^{-1}$ and clear right shoulders at 1100 and 1175 $cm^{-1}$. These clear right shoulders in this prealumina oxynitride glass should

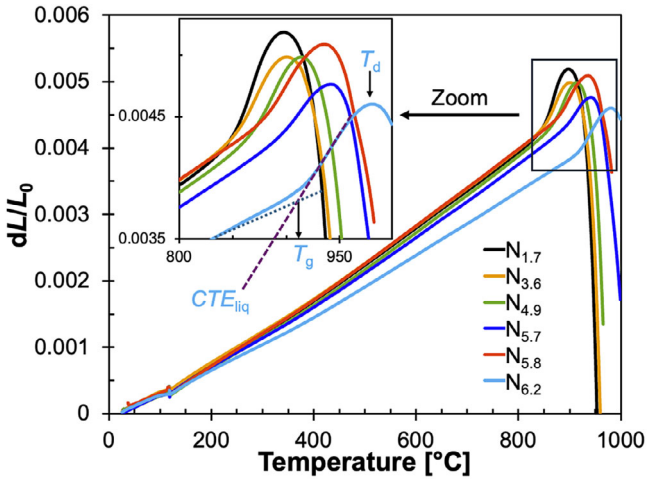


**FIGURE 2** Thermal expansion ($dL/L_0$) as a function of temperature. The inset indicates the measure of $T_g$, $CTE_{liq}$, and $T_d$.

be the results of the balance charge from the excess $Al^{3+}$ since in oxynitride glasses, some $Si^{4+}$ will form $SiO_3N$ units that requires the presence of an extra positive charge locally to balance the extra negative charge from the N anion (charge deficit), and with high Si content (as in this $N_{5.7}$ sample), there might also be the formation of $SiO_2N_2$, $SiON_3$, or even $SiN_4$ units.[71] On the contrary, $N_{6.2}$ sample, having the largest N and Al contents among the studied glasses, may also form the Al-N content with the presence of units with two or three nonbridging nitrogen ions ($N^{II}$ and $N^{I}$ coordinates, respectively). Therefore, the present peak is shifted to higher wavelength for the $N_{6.2}$ sample as seen in Figure 1. For similar reason, in the mid-frequency range (i.e., at 650–850 $cm^{-1}$ range), the main band centered at 790 $cm^{-1}$ for $N_{5.7}$ sample broadens and shifts to a lower frequency and is centered at 770 $cm^{-1}$ for the $N_{6.2}$ sample. In the low-frequency range, the main peak broadens and shifts to the higher frequency, from $N_{5.7}$ to $N_{6.2}$ glass samples. This observation suggests an increase in the $AlO_4$ unit, and a decrease in the Si-O-Si and Si-O-Al stretching vibrations. However, we could not conclude if there is any relation between these two changes. Further studies, such as NMR experiment, should be performed to have a clear understanding of these structural changes.

## 3.2 | Thermal and physical properties

The glass transition temperature ($T_g$) was determined from the thermal expansion curves (Figure 2) and is listed in Table 2. As expected, the $T_g$ of the studied oxynitride glasses increase monotonically with the N content in both prealkaline and prealumina glasses. For the per-alkaline glasses, $T_g$ increases from 843°C for $N_{1.7}$ sample to 875°C for $N_{5.8}$ sample. For the per-alumina glasses, $T_g$ increases from 887°C for $N_{5.7}$ sample to 916°C for $N_{6.2}$ sample. These increases in both cases may be explained by the fact that the increase of the N content leads to an increase of the dissociation energy, which is correlated to $T_g$.[72] Although the $N_{5.7}$ and $N_{5.8}$ samples have nearly the same N content, the $N_{5.7}$ sample, which has higher Al content (per-alumina glass), also exhibits a higher $T_g$. This is in agreement with previous findings.[73] The same trend can be seen in the case of dilatometric softening point ($T_d$) for both per-alumina and per-alkaline glasses (Table 1).

The thermal expansion curves are shown in Figure 2. Below $T_g$, the thermal expansion is almost linear. Nevertheless, two temperature ranges can be considered, 25–400°C ($CTE_{400}$) and 400–800°C ($CTE_{800}$), as shown in Table 2. In general, *CTE* increases with increasing glass modifier content (Mg in our case), and decreases with increasing the glass former content (Si in our case).[8,73] However, the per-alkaline glasses in our study do not show any significate variation in both $CTE_{400}$ and $CTE_{800}$. Moreover, in the per-alumina glasses, $N_{5.7}$ sample having lower Mg content than that of $N_{6.2}$ sample has the higher *CTE*. This contradictory may be caused by the increase of the N content, and the increase of $AlO_4$ units (see Section 3.1), which are known to result in the lower *CTE* of the oxynitride glasses.[2,73] Above $T_g$, the *CTE* of the supercooled liquid (namely, $CTE_{liq}$) can be determined from the curves as seen in the inset of Figure 2. For the per-alkaline glasses, it can be seen clearly that the $CTE_{liq}$ decreases with increasing the N content. In the per-alumina glasses, $CTE_{liq}$ increases with increasing the N content. More studies should be performed to have a clear relation between *CTE* and the oxynitride glass composition.

The glass density along with its accompanying molar volume and atomic packing density is shown in Table 2. Figure 3A plots $\rho$ against the N content of the studied glasses, revealing (i) concomitant increases of $\rho$ and N content withing per-alkaline and per-alumina glasses, (ii) the per-alkaline glasses exhibit higher densities than the per-alumina ones of similar N content, and (iii) the increase rate of densities with increasing N content of per-alumina glasses is greater than that of the per-alkaline ones (Figure 3A). To explain all these trends, we note that the increasing of Al content in the AlSiO glasses leads to the increase of glass densities as the density of amorphous alumina (3.05 g $cm^{-3}$) is greater than that of silica (2.2 g $cm^{-1}$).[63] In MgAlSiO glasses, the increase of Mg and Al contents leads to the great increase of the glass density, while the incorporation of the decrease of Al content into the increase of Mg content leads to the small increase of

**TABLE 2** Glass ID, thermal ($T_g$, *CTE*, and $T_d$), and physical ($\rho$, $V_M$, and $C_g$) properties.

| | Thermal properties[a] | | | | | Physical properties[b] | | |
|---|---|---|---|---|---|---|---|---|
| ID | $T_g$ [°C] | $CTE_{400}$ [$10^{-6}$°C $^{-1}$] | $CTE_{800}$ [$10^{-6}$°C $^{-1}$] | $CTE_{liq}$ [$10^{-6}$°C $^{-1}$] | $T_d$ [°C] | $\rho$ [g cm$^{-1}$] | $V_M$ [cm$^3$ mol$^{-1}$] | $C_g$ |
| $N_{1.7}$ | 843 | 4.3 | 5.6 | 25.2 | 898 | 2.65 | 7.60 | 0.526 |
| $N_{3.6}$ | 849 | 4.5 | 5.7 | 18.0 | 901 | 2.68 | 7.51 | 0.535 |
| $N_{4.9}$ | 866 | 4.3 | 5.6 | 17.3 | 915 | 2.72 | 7.41 | 0.544 |
| $N_{5.7}$ | 887 | 4.3 | 5.3 | 10.9 | 942 | 2.67 | 7.54 | 0.538 |
| $N_{5.8}$ | 875 | 4.4 | 5.7 | 14.8 | 937 | 2.78 | 7.24 | 0.557 |
| $N_{6.2}$ | 916 | 3.8 | 4.8 | 13.4 | 981 | 2.73 | 7.38 | 0.544 |

[a]The errors of $T_g$, *CTE*, and $T_d$ were ± 5°C, ± 0.1 × $10^{-6}$°$C^{-1}$, and ± 5°C, respectively.
[b]The uncertainty of $\rho$, $V_M$, and *C*g were ± 0.01 g cm$^{-1}$, ± 0.02 cm$^3$ mol$^{-1}$, and ± 0.001, respectively.

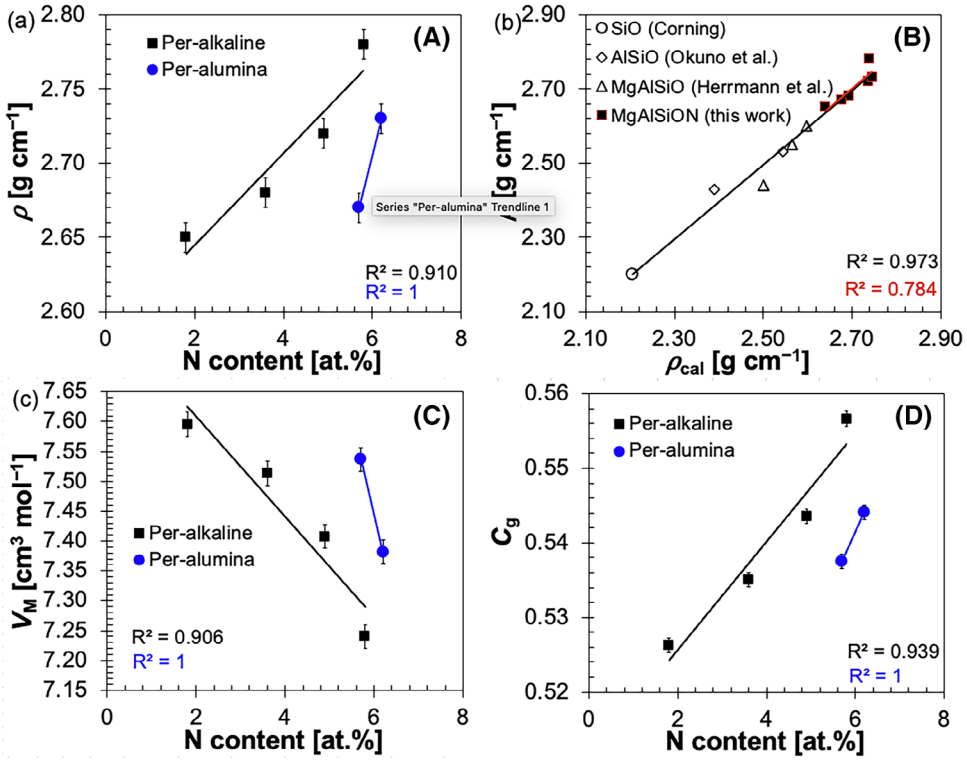


**FIGURE 3** Experimental values of (A and B) density, (C) molar volume, and (D) atomic packing density plotted against the N content (in at.%) of the MgAlSiON glasses, except for (B), which depicts the experimental density versus the one calculated ($\rho_{cal}$) from Equation (10). Black and blue symbols in (A, C, and D) represent data from per-alkaline and per-alumina glasses, respectively. SiO (silica glass), AlSiO, MgAlSiO, and MgAlSiON data are from Corning datasheet, Ref.[63] Ref. [76], and this work, respectively.

the glass density.[74] The preferable influence of Mg content is due to the fact that the density of an amorphous MgO (~3.40 g cm$^{-1}$) is greater than the one of either amorphous alumina or silica.[75] In oxynitride glasses, the increase of N content leads to the increase of density because of the more compacting structure of N-content glasses.[2] In this work (MgAlSiON glasses), the density of the per-alkaline glasses increases slightly with increasing the N content because in those glasses, the Mg content decreases at the same time (Table 1). For the per-alumina glasses, the density increases dramatically from $N_{5.7}$ to $N_{6.2}$ sample because both Mg and Al contents increase together with the increase of N content. To explain point (iii) above, we compare the $N_{1.7}$ and $N_{5.7}$ samples. $N_{1.7}$ sample, having similar Al and Si contents to those of $N_{5.7}$ sample, has the N content more than three times smaller than that of $N_{5.7}$ sample but has the Mg content less than twice greater than that of $N_{5.7}$ sample (Table 1). As both glasses have similar density value, we conclude that the influence of the Mg content increase is more than that of the N-content increase. Altogether, these glass-composition trends underlie the observed density range between 2.65 and 2.78 g cm$^{-1}$ (Table 2).

Our observed increase of density with increasing the N content mirrors that reported previously for several oxynitride glass systems.[2,28,51] However, the density does not increase linearly with the increase of N content or N/O ratio as seen in the different slope of per-alumina and per-alkaline glasses (Figure 3A). In fact, the density depends strongly on the masses of the glass constituents, whereas both the molar volume and the atomic packing density are also affected by the amounts of the elements involved in the oxynitride glass.[12,28,77,78] Hence, the glass density in this work was fitted using the ratios of N/O, Mg/Al, and Al/Si as the following:

$$\rho_{\text{cal}} = 1.971\,(\text{N/O}) + 0.349\,(\text{Mg/Al}) + 0.277\,(\text{Al/Si}) + 2.205\ \left(R^2 = 0.784\right), \quad (10)$$

where all the ratios are smaller than 1 and can be found in Table 1. The advantage of Equation (10) is that when there is no N content, it can be used to calculate the density of MgAlSiO glasses with a constraint that both Mg/Al and Al/Si ratios smaller than 1. When there is neither N nor Mg content, Equation (10) can be used to calculate the density of AlSiO glasses with a condition that Al/Si < 2. Moreover, if Al content = 0, then the calculated density of Equation (10) is equal to 2.205, which is the density of pure silica glass (i.e., the SiO glass). *The factors in front of the N/O, Mg/Al, and Al/Si ratios indicate the positive or negative impact of each ratio on the density. For instance, if we would like to decrease the density of an oxynitride glasses, it is more efficient to decrease the Mg/Al ratio (a factor of 0.349) rather than the Al/Si ratio (a factor of 0.277)*. In this sense, Equation (10) can be read as all the N/O, Mg/Al, and Al/Si ratios have the positive impact on the density, with the most (positive) impact for N/O and the less (positive) impact for Al/Si ratio. Figure 3B shows the correlation between the experimental density ($\rho$) and the calculated one ($\rho_{\text{cal}}$) obtained from Equation (10). Notably, even though the MgAlSiON glasses form this work used in the fitting process, the calculated densities of SiO, AlSiO, MgAlSiO, and these MgAlSiON glasses are in good agreement with the experimental ones.[63,76]

The molar volume and atomic packing density are plotted against the N content in Figure 3C and 3D, respectively. For both per-alkaline and per-alumina glasses, $V_{\text{M}}$ decreases, whereas $C_{\text{g}}$ increase with increasing the N content in the glass network. The atomic packing density ranges between 0.526 ($N_{1.7}$) and 0.557 ($N_{5.8}$), which are slightly greater (but in the same range as) than those of the CaAlSiON glasses with similar N content.[28]

## 3.3 | Mechanical properties

Table 3 shows the mechanical properties measured by ultrasonic echography (elastic moduli), indentation (hardness and crack resistance), and SEPB (fracture toughness) methods. As for the density and atomic packing density, the elastic moduli of the oxynitride glasses are known to also increase concomitantly with increasing N contents.[5,12,28,77] Moreover, the elastic properties of both oxide and oxynitride glasses depend on several structural parameters such as the cation–anion bond strengths, the atomic densities, and the glass-network connectivity.[48,51,79–81] The elastic properties increase with increasing the N content in the same way as those of $C_{\text{g}}$ (Tables 1 and 2), that is, within each per-alkali and per-alumina series (Figure 3 and 4). We first consider the Young's modulus, which ranges from 105 GPa for $N_{1.8}$ sample to 129 GPa for $N_{6.2}$ sample and reveals a good relation for each glass series ($R^2$ = 0.996 for per-alkali series). We note that sample $N_{5.7}$, having the same compactness ($C_{\text{g}}(N_{5.7})$ = 0.538) as the one of $N_{3.6}$ sample ($C_{\text{g}}(N_{3.6})$ = 0.535), possess $E$ higher than $N_{3.6}$ and even equal to that of the $N_{5.8}$ sample that has higher atomic packing density ($C_{\text{g}}(N_{5.8})$ = 0.557, Table 2). This can be explained by the fact that $N_{5.7}$ sample, having the highest Si content and relatively high N content, has the high network rigidity from the formation of $SiO_2N_2$, $SiON_3$, or even $SiN_4$ units (see Section 3.1).[71] Similar explanation goes to the $N_{6.2}$ sample, but this sample has the highest Al and N contents, which facilitates the formation of rigid glass-network structures such as $AlO_4$ unit instead of the less rigid structure such as the $AlO_5$ and $AlO_6$ units (see Section 3.1). The high E of these per-alumina glasses may also be the result of the low Mg content, in general, relative to the Al content. In fact, the overall best fit for both per-alkali and per-alumina glass series is the one that involves all Mg, Al, Si, and N contents as in Equation (11) as

$$E_{\text{cal}} = 267.4\,(\text{N/O}) + 11.2\,(\text{Mg/Al}) + 27.9\,(\text{Al/Si}) + 74.4\ \left(R^2 = 0.922\right), \quad (11)$$

where Mg/Al < 1 and Al/Si < 2 conditions should be met to have a good agreement between $E$ and $E_{\text{cal}}$ values. In this paper, we do not limit the O/N ratio as we have limited property data on MgAlSiON glass system to validate the derived regression model, particularly when the Mg/Al < 1 and Al/Si < 2 conditions are applied. However, we note that the current model has been validated up to an O/N = 0.112 (corresponding to an N content of 6.2 at %). From Equation (11), we see that all the three ratios have the positive impact on the Young's modulus, with the most impact for N/O ratio (267.4)

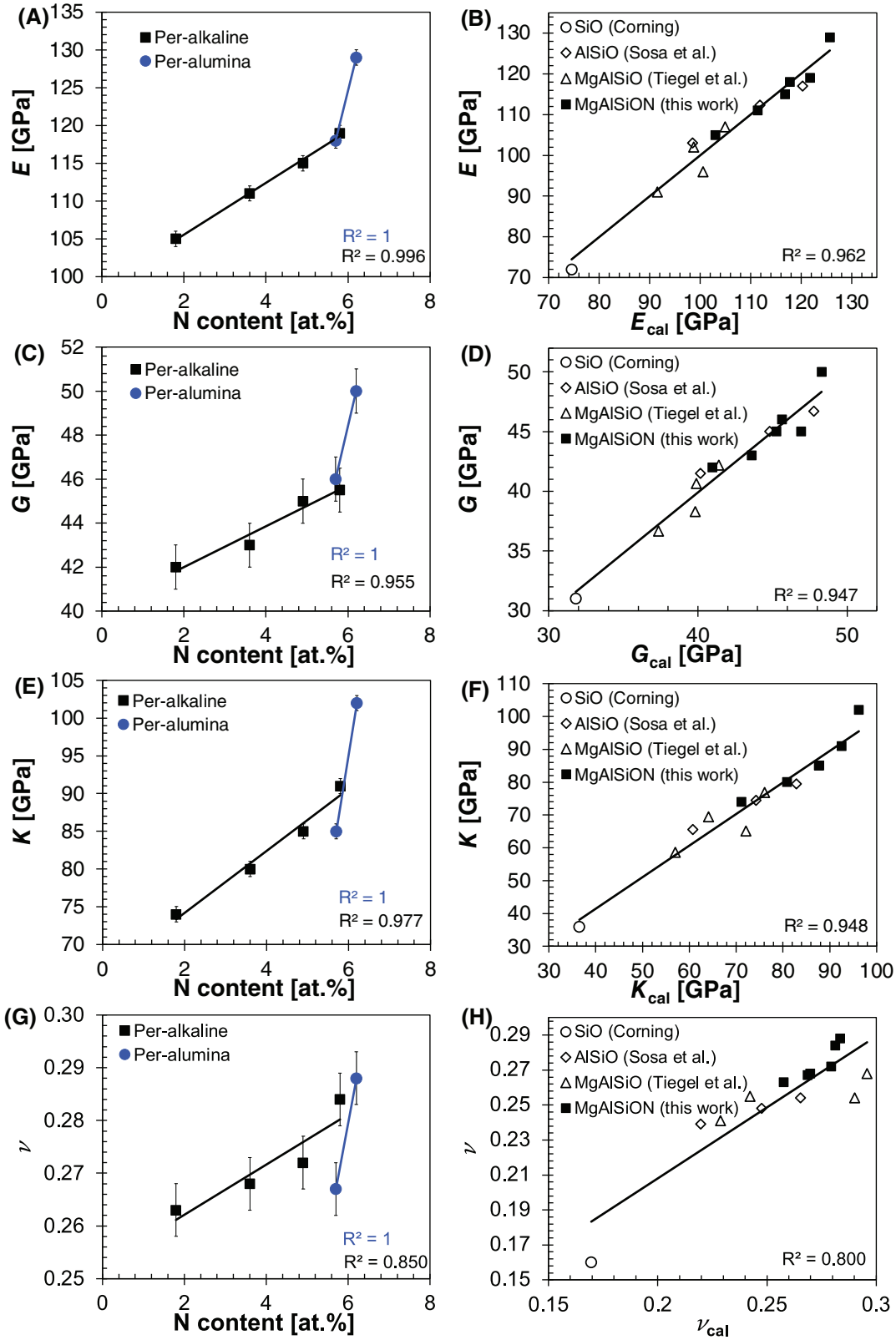


**FIGURE 4** Elastic moduli of the studied glasses against the N content and against the calculated values.

**TABLE 3** Glass ID, elastic moduli ($E$, $G$, $K$, $\nu$) hardness ($H_{load\text{-}ind}$), crack resistance ($CR$), and fracture toughness ($K_{Ic}$) of the MgAlSiON glasses.

| | | Ultrasonic echography[a] | | | Indentation and SEPB[b] | | |
|---|---|---|---|---|---|---|---|
| **ID** | ***E* [GPa]** | ***G* [GPa]** | ***K* [GPa]** | **$\nu$** | **$H_{load\text{-}ind}$ [GPa]** | ***CR* [N]** | **$K_{Ic}$ [MPa m$^{0.5}$]** |
| $N_{1.7}$ | 105 | 42 | 74 | 0.263 | 8.0 | 6.7 | 0.87 |
| $N_{3.6}$ | 111 | 43 | 80 | 0.268 | 8.6 | 2.1 | 0.93 |
| $N_{4.9}$ | 115 | 45 | 85 | 0.272 | 9.0 | 5.5 | 1.02 |
| $N_{5.7}$ | 118 | 46 | 85 | 0.267 | 9.6 | 2.3 | 1.37 |
| $N_{5.8}$ | 117 | 45 | 91 | 0.284 | 9.2 | 2.0 | 1.11 |
| $N_{6.2}$ | 129 | 50 | 102 | 0.288 | 9.8 | 3.6 | 1.59 |

[a]The error of $E$, $G$, and $K$ was ± 1 GPa and the error of $\nu$ was ± 0.005.

[b]The uncertainty of $H$, $CR$, and $K_{Ic}$ were ± 0.1 GPa, ± 0.2×$CR$ N, and ± 0.05, respectively.

and the less impact for Mg/Al ratio (11.2). This means that to increase the Young's modulus, it is enough to increase/add a small amount of N into the silica-based glasses. Equation (11) can also be applied to silicate, binary aluminosilicate, Mg-aluminosilicate, and oxynitride-Mg-aluminosilicate glasses as shown in Figure 4B ($R^2 = 0.962$). When there is no N content in the glass (in the case of MgAlSiO glass), Equation (11) depends on Mg/Al and Al/Si ratios, and when there is neither N and Mg (in the case of AlSiO glass), Equation (11) depends solely on Al/Si ratio. Lastly, if all N, Mg, and Al contents equal to zeros, $E_{cal} = 74.4$ GPa, which is the similar value of $E$ of the $SiO_2$ glass.

As revealed by Figure 4C,E, also the shear and bulk moduli increase linearly with N content within each glass series, as well as confirming additional enhancements of moduli for increasing Al/Si ratio as

$$G_{cal} = 84.1\,(N/O) + 3.2\,(Mg/Al) + 9.8\,(Al/Si) + 31.8\,\left(R^2 = 0.791\right), \quad (12)$$

$$K_{cal} = 316.6\,(N/O) + 17.4\,(Mg/Al) + 28.3\,(Al/Si) + 36.5\,\left(R^2 = 0.872\right), \quad (13)$$

where the constraints of Mg/Al < 1 and Al/Si < 2 applied for the best fit of calculated and experimented elastic properties of all MgAlSiON, MgAlSiO, and AlSiO glasses. For the bulk modulus, the coefficient for N/O ratio (= 316.6) is very high comparing to those of Al/Si and Mg/Al ratios, suggesting a higher impact of N content than for the shear and Young's moduli. This suggestion can be seen in Figure 4E, where $N_{5.7}$ sample has a slightly lower $K$ than that of $N_{5.8}$ sample, whereas in the case of $G$ and $E$, the two glass samples have nearly the same moduli values (Figure 4A,C). Lastly, we note that as for $E_{cal}$ using Equation (10), $G_{cal}$ and $K_{cal}$ using Equations (11) and (12) can also be applied to SiO, AlSiO, MgAlSiO, and MgAlSiON glasses ($R^2 > 0.945$ for both Equations (11) and (12)).

In contrast to the Young's modulus, Poisson's ratio relates more to the connectivity and compactness of the glass network rather than its rigidity.[80,82] However, the oxynitride glasses exhibit higher Poisson's ratio than that of their N-free glass counterparts.[48] As a result, the trend of Poisson's ratio (Figure 4G) as a function of N content looks similar to the one of $C_g$ (Figure 3D) than the other elastic properties. $N_{5.7}$ and $N_{3.6}$ samples have similar values of $C_g$ and $\nu$. As for the other elastic properties, the best fit of $\nu$ is also obtained from involving Mg, Al, and Si contents in the following Equation (14) as

$$\nu_{cal} = 0.441\,(N/O) + 0.067\,(Mg/Al) + 0.059\,(Al/Si) + 0.170\,\left(R^2 = 0.781\right), \quad (14)$$

where Mg/Al < 1 and Al/Si < 2 should be applied. As for the other elastic moduli, the three ratios have the positive impact of the Poisson's ratio with the most positive impact for N/O ratio. However, the Mg/Al ratio (0.067) has more positive impact on the Poisson's ratio comparing to the Al/Si one (0.059). Figure 4H shows a good agreement ($R^2 = 0.800$) between the calculated and experimented values of $\nu$ for all silica-based glasses. The present MgAlSiON glasses reveal a span of Poisson's ratio between 0.263 and 0.288 for $N_{1.7}$ and $N_{6.2}$ samples, respectively (Table 3).

Figure 5 shows the hardness parameters obtained by the Vickers indentation technique. At loads below 10 N, $H$ decreases as the load is increased for all the studied oxynitride glasses (Figure 5A), revealing the so-called indentation size effect (ISE).[83–85] $H$ reaches a plateau at a sufficient load (in our case 9.81 N). Among several models proposed to describe the ISE behavior, we use the one from Ref. [85], which proposed that there exists a minimum indentation load $P_{min}$ (specimen resistance) necessary to initiate plastic deformation, and the load-independent hardness ($H_{load\text{-}ind}$) is expressed as

$$H_{load-ind} = \frac{2\,(P_i - P_{min})}{d^2}, \quad (15)$$

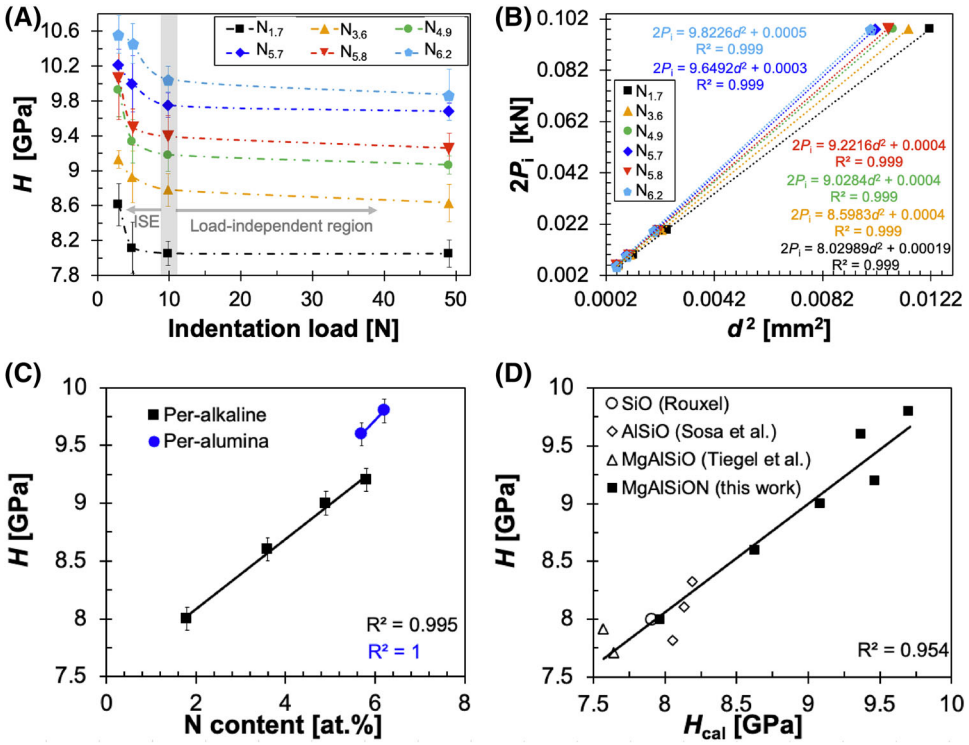


**FIGURE 5** (A) Hardness as a function of indentation load showing the indentation size effect (ISE). The dashed lines are guides for the eyes. (B) Applied indentation load as a function of indentation diagonal length squared according to the Hays–Kendall model. The dotted lines are obtained from linear fitting. (C) Hardness as a function of N content. (D) Experimental versus calculated hardness of **silica-based** glasses. The SiO (silica glass), AlSiO, MgAlSiO, and MgAlSiON data are from Refs. 87–89, and this work, respectively. We note that all the hardness values from the literature were also measured by Vickers indentation method at relatively high load to minimize the ISE.

where $P_i$ and $d$ are applied indentation load and indent diagonal length, respectively. From Equation (15), a plot of $2P_i$ against $d^2$ yields a straight line with $R^2 > 0.999$ (Figure 5B). This plot allows us to determine $P_{min}$ and $H_{load\text{-}ind}$ as summarized in Table 3 and Figure 5B. $H_{load\text{-}ind}$ ranges from 8.0 to 9.8 GPa for $N_{1.7}$ and $N_{6.2}$ glass samples, respectively. $P_{min}$ ranges from 0.1 to 0.25 N for $N_{1.7}$ and $N_{6.2}$ samples, respectively, and the range values are in good agreement to those of our previous work on borate-based glasses.[86] However, we note that the specimen resistance (i.e., $P_{min}$) of the present oxynitride glasses is higher than that of the borate-based glasses, which is logical. $H_{load\text{-}ind}$ ranges from 8.0 to 9.8 GPa for $N_{1.7}$ and $N_{6.2}$ glass samples, respectively.

Figure 5C shows the good agreement of the increase of hardness with increasing the N content for each glass series, that is, for per-alkali and per-alumina glasses ($R^2 \geq 0.995$). As for the elastic properties, a good fit can be obtained by getting involved the N/O, Mg/Al, and Al/Si ratios as in Equation (16) as

$$H_{cal} = 18.364\,(N/O) - 0.754\,(Mg/Al) + 0.173\,(Al/Si) + 7.905 \quad \left(R^2 = 0.959\right), \quad (16)$$

where Mg/Al < 1 and Al/Si < 2 should be applied to have a good fit ($R^2 = 0.959$). The increase of Mg/Al ratio leads to the decrease of hardness (negative impact), whereas the increase of N/O or Al/Si ratio increases the hardness (positive impact). The coefficient of N/O (18.364) of Equation (16) is much greater than those of Mg/Al and Al/Si ratios, suggesting the monotonic trend and according well with previous finding.[10,28,46] This finding reflects that the hardness is foremost governed by the cross-linking effects from N alone. Equation (16) can also be used for determining the calculated hardness of SiO, AlSiO, MgAlSiO, and MgAlSiON glasses (Figure 5D).

*CR* has been determined from the dependence of the probability of crack initiation on the applied indentation load as seen in Figure 6A. As expected, the crack probability increases with increasing the indentation load for all the studied glasses, but the onset load of the radial crack initiation differs from one another. With the indentation load of 2.94 N, the $N_{1.7}$, $N_{4.9}$, and $N_{6.2}$ samples have the crack probability less than 50%, whereas the one of the other three glasses (i.e., $N_{3.6}$, $N_{5.7}$, and $N_{5.8}$ samples) is greater than 50%. Therefore, the *CR* of the former three glass samples is greater than 2.94 N and the latter three glass samples smaller than 2.94 N as seen in Table 3. Figure 6B–E shows

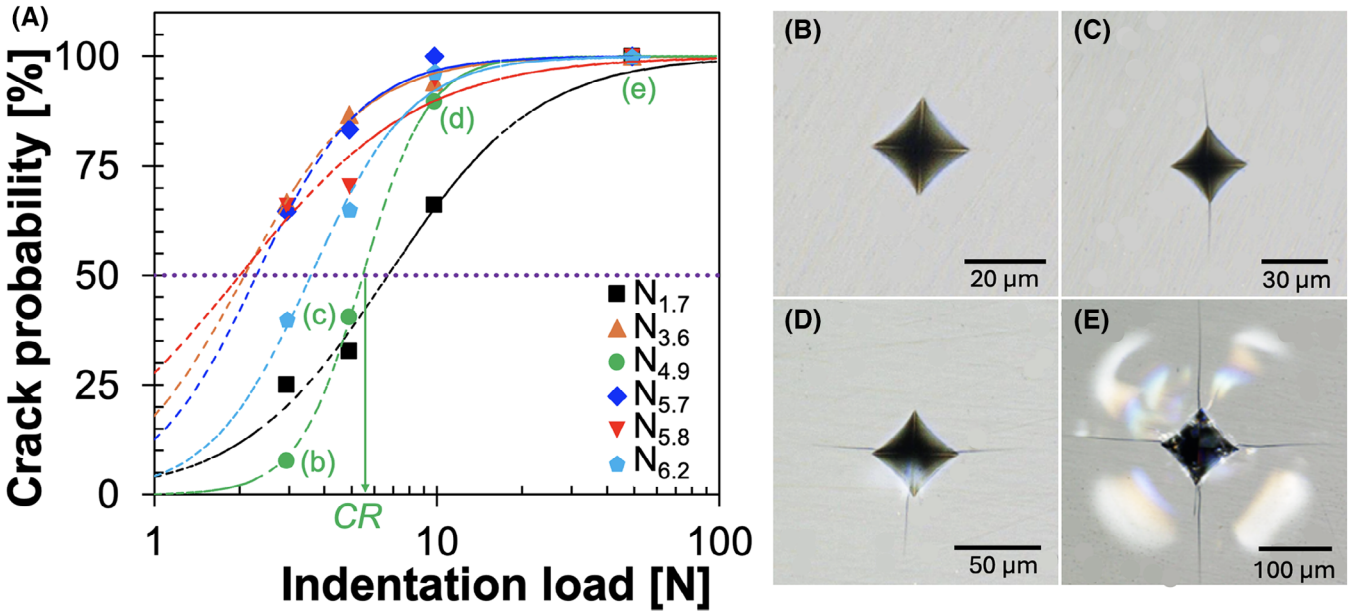


**FIGURE 6** (A) Crack probability as a function of indentation load of the six oxynitride glasses. (B)–(E) are the most-happening imprint of the indentation on the $N_{4.9}$ sample using the loads of 2.94, 4.91, 9.81, and 49.05 N, respectively.

the comparison of the Vickers imprints of the $N_{4.9}$ sample at different loads of 2.94–49.05 N as indicated in Figure 6A. For this $N_{4.9}$ sample, the four radial crack occurs all the time when the indentation load of 49.05 N was used (see Figure 6E). For the load of 2.94, 4.91, and 9.81 N, the most happening imprints (0, 2, and 3 corner cracks, respectively) are shown in Figure 6B, 6C, and 6D, respectively. To discuss the *CR* of the studied glasses, it is noteworthy that *CR* of a glass depends on several factors, in which the most important ones are the atomic packing density, the bond strength, and the glass connectivity.[61] As an example, $N_{1.7}$ and $N_{5.8}$ samples, having the lowest and the highest $C_g$ (0.516 and 0.557 in Table 2) among the studied glasses, are the most and the less crack-resistant, respectively (6.7 and 2.0 N in Table 3). $N_{3.6}$ and $N_{5.7}$ samples, having similar $C_g$ value (0.535 and 0.538, respectively) that is in between those of $N_{1.7}$ and $N_{5.8}$ samples, have the similar *CR* values of 2.1 and 2.3 N, respectively (Table 3). However, $C_g$ alone cannot explain the variation in *CR* of the studied glasses. N4.9 and N6.2 samples, having the same $C_g$ value of 0.544, show different *CR* of 5.5 and 3.6 N, respectively. To explain this variation, we first note that $N_{4.9}$ sample is the per-alkaline glass with the Mg/Al ratio of 0.714 similar to the one of $N_{1.7}$ sample, while $N_{6.2}$ sample is the per-alkaline glass with lower Mg/Al ratio of 0.458 (Table 1). The much amount of Mg content allows the $N_{4.9}$ (as well as $N_{1.7}$) sample to absorb the compressive energy from the indentation by bending the O-Mg-O angles.[61] On the contrary, $N_{6.2}$ sample, having high Al content (the highest Al/Si ratio as in Table 1) has a strong glass connectivity from the possible $Si(OAl)_z$ units (see Section 3.1 on glass structure), which may result in breaking the bond under high pressure as the indentation. In other words, the more connected glass network does not have space for the atomic movement, resulting in breaking the bond once the applying force/pressure is high enough.

Unlike *CR*, which is the crack initiation resistance of the glass surface, $K_{Ic}$ is the resistance to the unstable crack propagation of the bulk glass. In fact, a precrack or a flaw in a glass grows once the stress intensity factor from the applied force is larger than the $K_{Ic}$. $K_{Ic}$ has positive relation with bond strength, glass-network connectivity, and Young's modulus.[61] As a result, the increase of the N content increases directly the fracture toughness of the studied glasses (Figure 7A) because (1) the Si-N and Al-N bond strengths are greater than those of Si-O and Al-O ones, (2) $C_g$ increases with increasing the N content in both per-alkaline and per-alumina glasses (see Section 3.2), and (3) $E$ increases with increasing the N content (see previous section). For the per-alkaline glass samples, the fracture toughness increases from 0.87 to 1.11 MPa $m^{0.5}$ for $N_{1.7}$ and $N_{5.8}$ samples, respectively (Table 3). In the per-alumina glass samples, the crack needs to go throw the stronger bond of Si-O and Al-O (or Si-N and Al-N) rather than the relatively weaker bond of Mg-O. Together with the high Young's moduli, the per-alumina glass samples show higher crack-propagation resistance, that is, $K_{Ic}$ (1.37 and 1.59 MPa $m^{0.5}$ for $N_{5.7}$ and $N_{6.2}$ samples, respectively), comparing to those of the per-alumina glasses.

As for the other properties, a good fit for $K_{Ic}$ ($R^2 = 0.919$) can be obtained by getting involved the N/O, Mg/Al, and

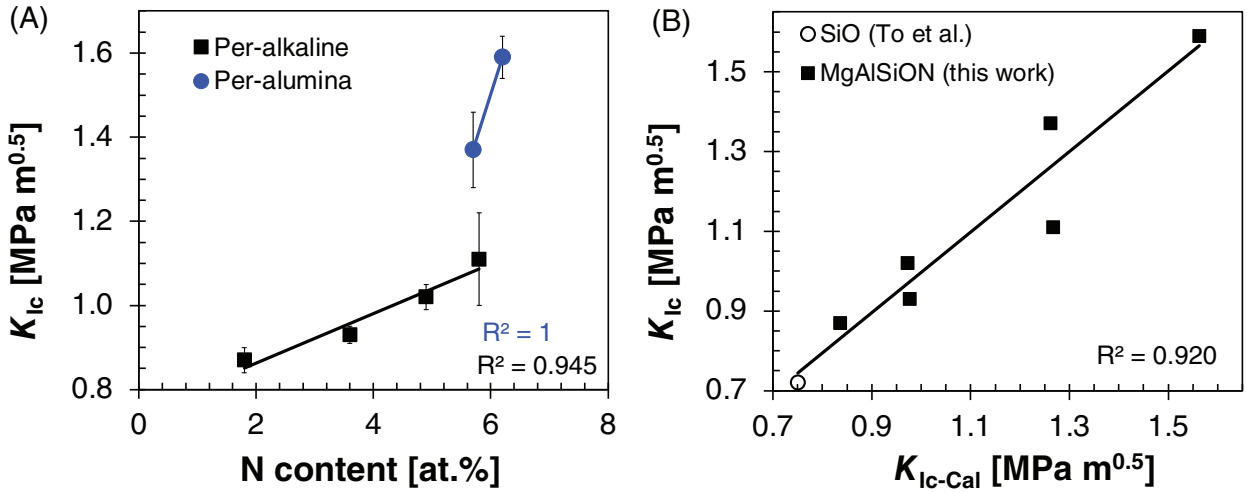


**FIGURE 7** (A) Fracture toughness as a function of N content. (B) Experimental versus calculated fracture toughness of silica and magnesium aluminosilicate glasses in this study.

Al/Si ratios as in Equation (17) as

$$K_{\mathrm{Ic\_cal}} = 3.632\,(\mathrm{N/O}) - 0.964\,(\mathrm{Mg/Al}) + 1.465\,(\mathrm{Al/Si}) + 0.750\,\left(R^2 = 0.919\right), \quad (17)$$

where Mg/Al < 1 and Al/Si < 2 should be applied to have the good fit ($R^2$ = 0.919). We note that the addition of Mg content (the negative sign in front of the 0.964 factor) decreases the $K_{\mathrm{Ic}}$, while the addition of both N and Al contents increases the $K_{\mathrm{Ic}}$. This observation has a good agreement with the argument in the previous paragraph of this section. Lastly, we note that there is no real relationship between the crack-initiation and crack-propagation resistance in the case study, which agrees well with Ref. 61. Figure 8 shows the relationship between *RC* (a measure for crack/flaw initiation resistance) and $K_{\mathrm{Ic}}$ (a measure for crack/flaw growth resistance) of MOF, chalcogenide, silicate, aluminoborate, aluminosilicate, aluminoborosilicate, and the present oxynitride glasses. MOF and chalcogenide glasses have the smallest $K_{\mathrm{Ic}}$ values, but they have relatively high *CR*. Aluminoborate glasses have the highest CR values, but they have the medium $K_{\mathrm{Ic}}$ comparing to the other glass family. Oxynitride glasses have the highest $K_{\mathrm{Ic}}$, while Borosilicate glasses have the lowest CR among the studied glasses. Again, there is no clear relationship between the crack initiation and growth resistance.

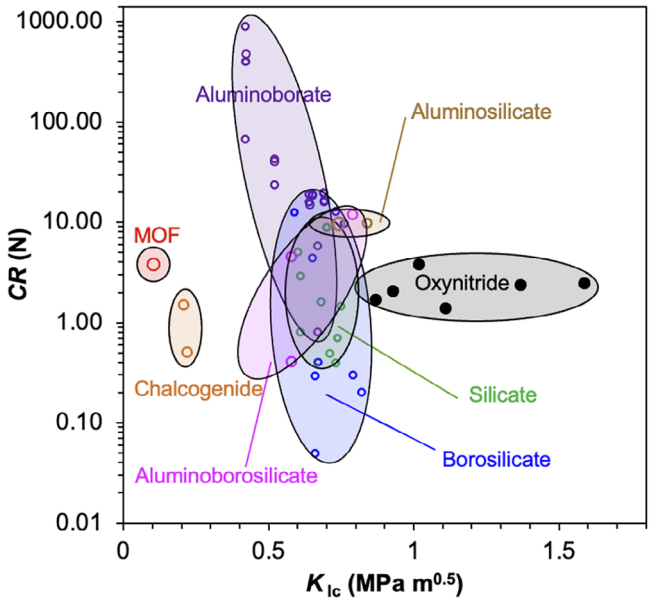


**FIGURE 8** Crack resistance (*CR*) versus fracture toughness ($K_{\mathrm{Ic}}$). This figure is adopted with data from Ref. 61 in addition to data for MOF glass[90] chalcogenide glasses,[91,92] aluminoborate glasses[93] and the present oxynitride glasses. All *CR* and $K_{\mathrm{Ic}}$ data are from the SEPB (CNB method only for chalcogenide glasses), and Vickers indentation, respectively, at temperature of 20–25°C and relative humidity of 50–60%.

## 4 | CONCLUSIONS

The structure, thermal, and mechanical properties, in particular the crack resistance and fracture toughness, of glasses from the Mg–Al–Si–O–N system with nitrogen contents up to 6.2 at % (equivalent to 14.4% of total anions) were studied. Structural characterization revealed that in the per-alkaline earth glasses (2Mg/Al > 1), the peaks shift to lower wavenumbers with decreasing Mg content (and increasing nitrogen), indicating substitution of $Al^{3+}$ for $Si^{4+}$ in the network. This is consistent with reduced force constants and increased Al–Si coupling. Furthermore, the decrease in Mg content leads to a reduction in the content

of BOs in $SiO_4$ units, likely stabilized by $Mg^{2+}$. In peralumina glasses (2Mg/Al < 1), the spectra are dominated by $SiO_3N$ and potentially $SiO_2N_2$ or $SiN_4$ units. In the case of sample N6.2 (which has the highest N and Al contents), the spectra reflect the formation of Al–N linkages (with $N^I$ and $N^{II}$ configurations) and a larger concentration of $AlO_4$ tetrahedra. Notably, the predominance of Si/Al $O_4$ tetrahedra and the strong preference for Si–N over Al–N bonds underpins the observed trends.

Density, compactness, hardness, elastic moduli, and fracture toughness increase with increasing nitrogen content, driven by enhanced network connectivity from $N^{3+}$-for-$O^{2-}$ substitution. However, these properties do not increase linearly with increasing the N content or the N/O ratio. In fact, the regression models for these properties showed strong agreement with experimental results when we involve N/O, Mg/Al, and Al/Si ratios, highlighting the critical role of each ratio in enhancing the properties. Moreover, with the constraints of Mg/Al < 1 and Al/Si < 2, the regression models could also be used to estimate the properties of MgAlSiO, AlSiO, and SiO glass systems. The models show that, unlike the other properties, hardness and fracture toughness decrease with increasing the Mg/Al ratio. Here, we would give the ranges for the MgAlSiON glasses. Young's modulus and hardness are in the [105 – 129] and [8 – 9.8] GPa ranges, respectively. $K_{Ic}$ is between 0.8 and 1.6 MPa $m^{0.5}$, with the optimum value being ~ 2.2 times the one of silica or soda–lime–silica glass for the $Mg_{5.5}Al_{12}Si_{20.7}O_{55.6}N_{6.2}$ composition.

## ACKNOWLEDGMENTS

We thank Corning Incorporated for providing some glass samples. Christophe Calers (UnivRen) were thanked for helping in EDS-SEM measurement.

## ORCID

*Theany To* https://orcid.org/0000-0002-8127-1579
*Sharafat Ali* https://orcid.org/0000-0003-1430-2862
*Karolina Milewska* https://orcid.org/0000-0003-0676-5082

## REFERENCES

1. Ali S, Jonson B, Pomeroy MJ, Hampshire S. Issues associated with the development of transparent oxynitride glasses. Ceram Int. 2015;41(3, Part A):3345–54. https://doi.org/10.1016/j.ceramint.2014.11.030
2. Duval A, Houizot P, Rouxel T. Review: elaboration, structure, and mechanical properties of oxynitride glasses. J Amer Ceram Soc. 2023;106(3):1611–37. https://doi.org/10.1111/JACE.18824
3. Sakka S. Structure, properties and application of oxynitride glasses. J Non-Crystal Solids. 1995;181(3):215–24. https://doi.org/10.1016/S0022-3093(94)00514-1
4. Hampshire S, Drew RAL, Jack KH. Oxynitride glasses. Phys Chem Glasses. 1985;26(5):182–86.
5. Hampshire S. Oxynitride glasses. J Eur Ceram Soc. 2008;28(7):1475–83. https://doi.org/10.1016/j.jeurceramsoc.2007.12.021
6. Hampshire S, Drew RAL, Jack KH. Viscosities, glass transition temperatures, and microhardness of Y-Si-A1-O-N glasses. J Am Ceram Soc. 1984;67(3):C–46–C–47. https://doi.org/10.1111/j.1151-2916.1984.tb19752.x
7. Lofaj F, Dériano S, LeFloch M, Rouxel T, Hoffmann MJ. Structure and rheological properties of the RE–Si–Mg–O–N (RE = Sc, Y, La, Nd, Sm, Gd, Yb and Lu) glasses. J Non-Crystal Solids. 2004;344(1):8–16. https://doi.org/10.1016/j.jnoncrysol.2004.07.018
8. Lofaj F, Satet R, Hoffmann MJ, de Arellano López AR. Thermal expansion and glass transition temperature of the rare-earth doped oxynitride glasses. J Eur Ceram Soc. 2004;24(12):3377–85. https://doi.org/10.1016/j.jeurceramsoc.2003.10.012
9. Messier DR, Gleisner RP. Preparation and characterization of Li-Si-Al-O-N glasses. J Amer Ceram Soc. 1988;71(6):422–25. https://doi.org/10.1111/j.1151-2916.1988.tb05888.x
10. Paraschiv GL, Gomez S, Mauro JC, Wondraczek L, Yue Y, Smedskjaer MM. Hardness of oxynitride glasses: topological origin. J Phys Chem B. 2015;119(10):4109–15. https://doi.org/10.1021/jp512235t
11. Rocherulle J, Guyader J, Verdier P, Laurent Y. Li-Si-Al-O-N and Li-Si-O-N oxynitride glasses study and characterization. J Mater Sci. 1989;24(12):4525–30. https://doi.org/10.1007/BF00544539
12. Rouxel T, Dély N, Sangleboeuf JC, Dériano S, LeFloch M, Beuneu B, et al. Structure–property correlations in Y–Ca–Mg–sialon glasses: physical and mechanical properties. J Am Ceram Soc. 2005;88(4):889–96. https://doi.org/10.1111/j.1551-2916.2005.00146.x
13. Rouxel T, Huger M, Besson JL. Rheological properties of Y-Si-Al-O-N glasses — elastic moduli, viscosity and creep. J Mater Sci. 1992;27(1):279–84. https://doi.org/10.1007/BF00553867
14. Ali S, Jonson B. Compositional effects on the properties of high nitrogen content alkaline-earth silicon oxynitride glasses, AE = Mg, Ca, Sr, Ba. J Eur Ceram Soc. 2011;31(4):611–18. https://doi.org/10.1016/j.jeurceramsoc.2010.11.005
15. Murakami Y, Yamamoto H. Properties of oxynitride glasses in the ln-Si-Al-O-N systems (Ln = rare-earth). J Ceram Soc Japan. 1994;102(1183):231–36. https://doi.org/10.2109/jcersj.102.231
16. Hampshire S, Pomeroy MJ. Effect of composition on viscosities of rare earth oxynitride glasses. J Non-Crystal Solids. 2004;344(1):1–7. https://doi.org/10.1016/j.jnoncrysol.2004.07.027
17. Jin J, Yoko T, Miyaji F, Sakka S, Fukunaga T, Misawa M. Neutron diffraction study on the structure of Na-Si-O-N oxynitride glasses. J Am Ceram Soc. 1993;76(3):630–34. https://doi.org/10.1111/j.1151-2916.1993.tb03652.x
18. Jin J, Yoko T, Miyaji F, Sakka S, Fukunaga T, Misawa M. Neutron diffraction and solid-state MAS-NMR studies of the structure of Y-AI-Si-O-N oxynitride glasses. Philos Mag B. 1994;70(2):191–203. https://doi.org/10.1080/01418639408241800
19. Uhlig H, Hoffmann M-J, Steeb S. Atomic structure of rare earth Si-Al-O-N glasses. Z Naturforschung A. 1998;53(5):259–64. https://doi.org/10.1515/zna-1998-0524
20. Videau JJ, Etourneau J, Rocherulle J, Verdier P, Laurent Y. Structural approach of sialon glasses: M-Si-Al-O-N. J Eur Ceram

Soc. 1997;17(15):1955–61. https://doi.org/10.1016/S0955-2219(97)00065-4
21. McMillan PF, Sato RK, Poe BT. Structural characterization of Si–Al–O–N glasses. J Non-Crystal Solids. 1998;224(3):267–76. https://doi.org/10.1016/S0022-3093(97)00468-7
22. Lemercier H, Rouxel T, Fargeot D, Besson J-L, Piriou B. Yttrium SiAlON glasses: structure and mechanical properties—elasticity and viscosity. J Non-Crystal Solids. 1996;201(1):128–45. https://doi.org/10.1016/0022-3093(96)00147-0
23. Dolekcekic E, Pomeroy MJ, Hampshire S. Structural characterisation of Er–Si–Al–O–N glasses by raman spectroscopy. J Eur Ceram Soc. 2007;27(2):893–98. https://doi.org/10.1016/j.jeurceramsoc.2006.04.058
24. Brow RK, Pantano CG, Boyd DC. Nitrogen coordination in oxynitride glasses. J Am Ceram Soc. 1984;67(4):c72–c74. https://doi.org/10.1111/j.1151-2916.1984.tb18834.x
25. Schneider M, Gasparov VA, Richter W, Deckwerth M, Rüssel C. XPS studies on oxynitride glasses in the system Si-Al-O-N. J Non-Crystal Solids. 1997;215(2):201–7. https://doi.org/10.1016/S0022-3093(97)00076-8
26. Deckwerth M, Rüssel C, Schneider M, Richter W, Hirsch O, Gerald K-F, *et al.* Spectroscopic characterisation of oxynitride glasses in the system Mg–Ca–Si–Al–O–N. Phys Chem Glasses. 2001;42(2):88–94.
27. Ali S, Ryl J, Hakeem AS, Grochowska K, Wójcik NA. Investigation of the structural and thermal properties of aluminum-rich Ca–Al–Si–O–N glasses. Progr Solid State Chem. 2023;71:100414. https://doi.org/10.1016/j.progsolidstchem.2023.100414
28. Ali S, Ellison A, Luo J, Edén M. Composition–structure–property relationships of transparent Ca–Al–Si–O–N oxynitride glasses: the roles of nitrogen and aluminum. J Am Ceram Soc. 2023;106(3):1748–65. https://doi.org/10.1111/jace.18866
29. Leonova E, Hakeem AS, Jansson K, Stevensson B, Shen Z, Grins J, et al. Nitrogen-rich La–Si–Al–O–N oxynitride glass structures probed by solid state NMR. J Non-Crystal Solids. 2008;354(1):49–60. https://doi.org/10.1016/j.jnoncrysol.2007.07.027
30. Hater W, Müller-Warmuth W, Frisch GH. 29Si MAS NMR studies of alkali silicate oxynitride glasses. Glastech Ber. 1989;62(9):328–34.
31. Aujla RS, Leng-ward G, Lewis MH, Seymour EFW, Styles GA, West GW. An NMR study of silicon coordination in Y–Si–Al–O–N glasses. Philos Mag B. 1986;54(2):L51–L56. https://doi.org/10.1080/13642818608239002
32. Engelhardt G, Michel D. High-resolution solid-state NMR of silicates and zeolites. Chichester: Wiley; 1987.
33. Ali S, Paul B, Magnusson R, Erik E, Camille P, Bo J, et al. Optical and mechanical properties of amorphous Mg-Si-O-N thin films deposited by reactive magnetron sputtering. Surface Coatings Technol. 2019;372:9–15. https://doi.org/10.1016/j.surfcoat.2019.05.015
34. Geyer V, Rüssel C. Oxinitride glasses in the system Mg-Al-Si-O-N, prepared with the aid of an electrochemically derived polymeric precursor. J Non-Crystal Solids. 1992;149(3):196–202. https://doi.org/10.1016/0022-3093(92)90067-T
35. Homeny J, Paulik SW. High-pressure synthesis of Mg-Al-Si-O-N oxynitride glasses. Mater Lett. 1990;9(12):504–7. https://doi.org/10.1016/0167-577X(90)90096-5
36. Homeny J, McGarry DL. Preparation and mechanical properties of Mg-Al-Si-O-N glasses. J Am Ceram Soc. 1984;67(11):c225–27. https://doi.org/10.1111/j.1151-2916.1984.tb19489.x
37. Sharafat A. "Preparation, characterization and properties of nitrogen rich glasses in alkaline earth-Si-O-N systems"; Ph.D. Thesis, Stockholm University, Stockholm, Sweden, 2009.
38. Shaw TM, Thomas G, Loehman RE. Formation and microstructure of Mg-Si-O–N glasses. J Am Ceram Soc. 1984;67(10):643–47. https://doi.org/10.1111/j.1151-2916.1984.tb19674.x
39. Sharafat A, Forslund B, Grins J, Esmaeilzadeh S. Formation and properties of nitrogen-rich strontium silicon oxynitride glasses. J Mater Sci. 2009;44(2):664–70. https://doi.org/10.1007/s10853-008-3058-3
40. Pastuszak R, Verdier P. M-Si-Al-O-N glasses (M = Mg, Ca, Ba, Mn, Nd), existence range and comparative study of some properties. J Non-Crystal Solids. 1983;56(1):141–46. https://doi.org/10.1016/0022-3093(83)90459-3
41. Tredway WK, Risbud SH. Melt processing and properties of barium-sialon glasses. J Am Ceram Soc. 1983;66(5):324–27. https://doi.org/10.1111/j.1151-2916.1983.tb10041.x
42. Ali S, Jonson B. Glasses in the Ba–Si–O–N system. J Am Ceram Soc. 2011;94(9):2912–17. https://doi.org/10.1111/j.1551-2916.2011.04718.x
43. Sharafat A, Grins J, Esmaeilzadeh S. Glass-forming region in the Ca–Si–O–N system using $CaH_2$ as Ca source. J Eur Ceram Soc. 2008;28(14):2659–64. https://doi.org/10.1016/j.jeurceramsoc.2008.04.017
44. Ali S. Elastic properties and hardness of mixed alkaline earth silicate oxynitride glasses. Materials. 2022;15(14):5022. https://doi.org/10.3390/ma15145022
45. Hakeem AS, Grins J, Esmaeilzadeh S. La–Si–O–N glasses: part I. Extension of the glass forming region. J Eur Ceram Soc. 2007;27(16):4773–81. https://doi.org/10.1016/j.jeurceramsoc.2007.04.002
46. Sharafat A, Grins J, Esmaeilzadeh S. Hardness and refractive index of Ca–Si–O–N glasses. J Non-Crystal Solids. 2009;355(4):301–4. https://doi.org/10.1016/j.jnoncrysol.2008.11.019
47. Gueguen Y, Sharafat A, Grins J, Rouxel T. Viscosity of high-nitrogen content Ca–Si–O–N glasses. J Eur Ceram Soc. 2010;30(16):3455–58. https://doi.org/10.1016/j.jeurceramsoc.2010.07.039
48. Sellappan P, Sharafat A, Keryvin V, Houizot P, Rouxel T, Grins J, et al. Elastic properties and surface damage resistance of nitrogen-rich (Ca, Sr)-Si-O-N glasses. J Non-Crystal Solids. 2010;356(41):2120–26.
49. Ali S. Impact of the atomic packing density on the properties of nitrogen-rich calcium silicate oxynitride glasses. Materials. 2022;15(17):6054. https://doi.org/10.3390/ma15176054
50. Sharafat A, Grins J, Esmaeilzadeh S. Properties of high nitrogen content mixed alkali earth oxynitride glasses $(AE_xCa_{1-x})_{1.2(1)}SiO_{1.9(1)}N_{0.86(6)}$, $AE$ = Mg, Sr, Ba. J Non-Crystal Solids. 2009;355(22):1259–63. https://doi.org/10.1016/j.jnoncrysol.2009.04.036
51. Loehman RE. Preparation and properties of oxynitride glasses. J Non-Crystal Solids. 1983;56(1):123–34. https://doi.org/10.1016/0022-3093(83)90457-X
52. Makishima A, Mitomo M, Ii N, Tsutsumi M. Microhardness and transparency of an La-Si-O-N oxynitride glass. J Am

Ceram Soc. 1983;66(3):C–55–C–56. https://doi.org/10.1111/j.1151-2916.1983.tb10037.x

53. Sakka S. Oxynitride glasses. Ann Rev Mater Res. 1986;16:29–46. https://doi.org/10.1146/annurev.ms.16.080186.000333
54. Leng-Ward G, Lewis MH. Oxynitride glasses and their glass-ceramic derivatives. In: Lewis MH, editor. Glasses and glass-ceramics. Dordrecht: Springer Netherlands; 1989. p. 106–55. https://doi.org/10.1007/978-94-009-0817-8_4
55. O'Meara C, Dunlop GL, Pompe R. Formation, crystallisation and oxidation of selected glasses in the Y-Si-Al-O-N system. J Eur Ceram Soc. 1991;8(3):161–70. https://doi.org/10.1016/0955-2219(91)90070-G
56. Ohashi M, Hampshire S. Formation of Ce-Si-O-N glasses. J Am Ceram Soc. 1991;74(8):2018–20. https://doi.org/10.1111/j.1151-2916.1991.tb07827.x
57. Pomeroy MJ, Hampshire S. SiAlON glasses: effects of nitrogen on structure and properties. J Ceram Soc Japan. 2008;116(1354):755–61. https://doi.org/10.2109/jcersj2.116.755
58. Shannon RD. Revised effective ionic radii and systematic studies of interatomic distances in halides and chalcogenides. Acta Crystallograph Sect A. 1976;32(5):751–67. https://doi.org/10.1107/S0567739476001551
59. Wada M, Furukawa H, Fujita K. Crack resistance of glass on Vickers indentation. Proc Int Congr Glass. 1974;11:39–46.
60. To T, Célarié F, Roux-Langlois C, Bazin A, Gueguen Y, Orain H, et al. Fracture toughness, fracture energy and slow crack growth of glass as investigated by the Single-Edge precracked Beam (SEPB) and Chevron-Notched Beam (CNB) methods. Acta Materialia. 2018;146:1–11. https://doi.org/10.1016/j.actamat.2017.11.056
61. To T, Jensen LR, Smedskjaer MM. On the relation between fracture toughness and crack resistance in oxide glasses. J Non-Crystal Solids. 2020;534:119946. https://doi.org/10.1016/j.jnoncrysol.2020.119946
62. ASTM C1421-10. Standard test methods for determination of fracture toughness of advanced ceramics at ambient temperature. West Conshohocken, PA: ASTM International; 2010
63. Okuno M, Zotov N, Schmücker M, Schneider H. Structure of $SiO_2$–$Al_2O_3$ glasses: combined X-ray diffraction, IR and Raman studies. J Non-Crystal Solids. 2005;351(12–13):1032–38. https://doi.org/10.1016/j.jnoncrysol.2005.01.014
64. Neuville DR, Cormier L, Montouillout V, Florian P, Millot F, Rifflet J, et al. Amorphous materials: properties, structure, and durability: structure of Mg- and Mg/Ca aluminosilicate glasses: 27Al NMR and Raman spectroscopy investigations. Am Mineralogist. 2008;93(11–12):1721–31. https://doi.org/10.2138/am.2008.2867
65. McMillan P, Piriou B. The structures and vibrational spectra of crystals and glasses in the silica-alumina system. J Non-Crystal Solids. 1982;53(3):279–98. https://doi.org/10.1016/0022-3093(82)90086-2
66. Seifert FA, Mysen BO, Virgo D. Three-dimensional network structure of quenched melts (glass) in the systems $SiO_2$-$NaAlO_2$, $SiO_2$-$CaAl_2O_4$ and $SiO_2$-$MgAl_2O_4$. Am Mineralogist. 1982;67(7–8):696–717.
67. Neuville DR, Mysen BO. Role of aluminium in the silicate network: In situ, high-temperature study of glasses and melts on the join $SiO_2$-$NaAlO_2$. Geochim Cosmochim Acta. 1996;60(10):1727–37. https://doi.org/10.1016/0016-7037(96)00049-X
68. Mysen BO, Virgo D, Seifert FA. Relationships between properties and structure of aluminosilicate melts. Am Mineralogist. 1985;70(1–2):88–105.
69. McMillan PF, Poe BT, Gillet PH, Reynard B. A study of $SiO_2$ glass and supercooled liquid to 1950 K via high-temperature raman spectroscopy. Geochim Cosmochim Acta. 1994;58(17):3653–64. https://doi.org/10.1016/0016-7037(94)90156-2
70. Taylor WR. Application of infrared spectroscopy to studies of silicate glass structure: examples from the melilite glasses and the systems $Na_2O$-$SiO_2$ and $Na_2O$-$Al_2O_3$-$SiO_2$. Proc Indian Acad Sci (Earth Planet Sci). 1990;99(1):99–117. https://doi.org/10.1007/BF02871899
71. Hakeem AS, Daucé R, Leonova E, Edén M, Shen Z, Grins J, et al. Silicate glasses with unprecedented high nitrogen and electropositive metal contents obtained by using metals as precursors. Adv Mater. 2005;17(18):2214–16. https://doi.org/10.1002/adma.200500715
72. Rouxel T. What we can learn from crystals about the mechanical properties of glass. J Ceram Soc Japan. 2022;130(8):519–30. https://doi.org/10.2109/jcersj2.22067
73. Ali S, Wójcik NA, Hakeem AS, Gueguen Y, Karlsson S. Effect of composition on the thermal properties and structure of M-Al-Si-O-N glasses, M = Na, Mg, Ca. Progr Solid State Chem. 2024;74:100461. https://doi.org/10.1016/j.progsolidstchem.2024.100461
74. Hermansen C, Guo X, Youngman RE, Mauro JC, Smedskjaer MM, Yue Y. Structure-topology-property correlations of sodium phosphosilicate glasses. J Chem Phys. 2015;143(6):064510. https://doi.org/10.1063/1.4928330
75. Bookwala M, DeBoyace K, Buckner IS, Wildfong PLD. Predicting density of amorphous solid materials using molecular dynamics simulation. AAPS PharmSciTech. 2020;21(3):96. https://doi.org/10.1208/s12249-020-1632-4
76. Herrmann A, Rüssel C. New aluminosilicate glasses as high-power laser materials. Int J of Appl Glass Sci. 2015;6(3):210–19. https://doi.org/10.1111/ijag.12127
77. Becher PF, Hampshire S, Pomeroy MJ, Hoffmann MJ, Lance MJ, Satet RL. An overview of the structure and properties of silicon-based oxynitride glasses. Int J Appl Glass Sci. 2011;2(1):63–83. https://doi.org/10.1111/j.2041-1294.2011.00042.x
78. Sakka S. Structure and properties of $Ga_2O_3$ based glasses. Trans Indian Ceram Soc. 2014;55(2):35–41. https://doi.org/10.1080/0371750X.1996.10804746
79. Sakka S, Kamiya K, Yoko T. Preparation and properties of Ca-Al-Si-O-N oxynitride glasses. J Non-Crystal Solids. 1983;56(1):147–52. https://doi.org/10.1016/0022-3093(83)90460-X
80. Rouxel T. Elastic properties and short-to medium-range order in glasses. J Am Ceram Soc. 2007;90(10):3019–39. https://doi.org/10.1111/J.1551-2916.2007.01945.X
81. Ecolivet C, Verdier P. Proprietes elastiques et indices de refraction de verres azotes. Mater Res Bull. 1984;19(2):227–31. https://doi.org/10.1016/0025-5408(84)90094-1
82. To T, Gamst C, Østergaard MB, Jensen LR, Smedskjaer MM. Fracture energy of high-Poisson's ratio oxide glasses. J Appl Phys. 2022;131(24):. https://doi.org/10.1063/5.0096855
83. Gong J, Miao H, Zhao Z, Guan Z. Load-dependence of the measured hardness of Ti(C,N)-based cermets. Mater Sci Eng. 2001;303(1–2):179–86. https://doi.org/10.1016/S0921-5093(00)01845-1

84. Şahin O, Uzun O, Kölemen U, Uçar N. Dynamic hardness and reduced modulus determination on the (001) face of $\beta$-Sn single crystals by a depth sensing indentation technique. J Phys Condensed Matter. 2007;19(30):306001. https://doi.org/10.1088/0953-8984/19/30/306001
85. Hays C, Kendall EG. An analysis of Knoop microhardness. Metallography. 1973;6(4):275–82. https://doi.org/10.1016/0026-0800(73)90053-0
86. To T, Ladjani I, Houizot P, Le Coq D, Calvez L, Moreac A, et al. Mechanical and electrochemical properties of lithium aluminoborate glasses. Glass Europe. 2024;2:27–44. https://doi.org/10.52825/glass-europe.v2i.1382
87. Rouxel T. Some strange things about the mechanical properties of glass. C R Phys. 2023;24(S1):99–112. https://doi.org/10.5802/crphys.126
88. Rosales-Sosa GA, Masuno A, Higo Y, Inoue H. Crack-resistant $Al_2O_3$-$SiO_2$ glasses. Sci Rep. 2016;6(1):23620. https://doi.org/10.1038/srep23620
89. Tiegel M, Hosseinabadi R, Kuhn S, Herrmann A. R??Ssel C. Young's modulus, Vickers hardness and indentation fracture toughness of alumino silicate glasses. Ceram Int. 2015;41(6):7267–75. https://doi.org/10.1016/j.ceramint.2015.01.144
90. To T, Sørensen SS, Stepniewska M, Qiao A, Jensen LR, Bauchy M, et al. Fracture toughness of a metal–organic framework glass. Nat Commun. 2020;11(1):1–9. https://doi.org/10.1038/s41467-020-16382-7
91. Guin J-P, Rouxel T, Sanglebœuf J-C, Melscoët I, Lucas J. Hardness, toughness, and scratchability of germanium–selenium chalcogenide glasses. J Am Ceram Soc. 2002;85(6):1545–52. https://doi.org/10.1111/j.1151-2916.2002.tb00310.x
92. Rouxel T. Fracture surface energy and toughness of inorganic glasses. Scripta Materialia. 2017;137:109–13.
93. To T, Pedersen CR, Gamst C, Andersen MH, Jensen LR, Smedskjaer MM. Mechanical properties of hydrated cesium-lithium aluminoborate glasses. Phys Rev Mater. 2021;5:83605. https://doi.org/10.1103/PhysRevMaterials.5.083605


**How to cite this article:** To T, Mhamdia C, Ali S, Houizot P, Milewska K, Tessier F, et al. Thermal and mechanical properties of Mg–Al–Si–O–N glasses with up to 6.2 at.% nitrogen. J Am Ceram Soc. 2025;e20487. https://doi.org/10.1111/jace.20487